technologies

Article

Fabrication and Characterization of $SnCl_2$- and CuBr-Added Perovskite Photovoltaic Devices

Yugo Asakawa [1], Takeo Oku [1,*], Masashi Kido [1], Atsushi Suzuki [1], Riku Okumura [1], Masanobu Okita [2], Sakiko Fukunishi [2], Tomoharu Tachikawa [2] and Tomoya Hasegawa [2]

[1] Department of Materials Science, The University of Shiga Prefecture, 2500 Hassaka, Hikone 522-8533, Shiga, Japan
[2] Osaka Gas Chemicals Co., Ltd., 5-11-61 Torishima, Konohana-ku, Osaka-shi 554-0051, Osaka-fu, Japan
* Correspondence: oku@mat.usp.ac.jp; Tel.: +81-749-28-8368

Abstract: Perovskite photovoltaic devices added with tin (Sn) dichloride and copper (Cu) bromide were fabricated and characterized. The thin film devices were prepared by an ordinary spin-coating technique using an air blowing method in ambient air. A decaphenylcyclopentasilane layer was coated at the surface of perovskite layer and annealed at a high temperature of 190 °C. Conversion efficiencies and short-circuit current densities were improved for devices added with Sn and Cu compared with the standard devices. The energy gap of the perovskite crystal decreased through the Sn addition, which was also confirmed by first-principles calculations.

Keywords: perovskite; solar cell; copper; tin; first-principles calculation; polysilane

check for updates

Citation: Asakawa, Y.; Oku, T.; Kido, M.; Suzuki, A.; Okumura, R.; Okita, M.; Fukunishi, S.; Tachikawa, T.; Hasegawa, T. Fabrication and Characterization of $SnCl_2$- and CuBr-Added Perovskite Photovoltaic Devices. *Technologies* **2022**, *10*, 112. https://doi.org/10.3390/technologies10060112

Academic Editor: Manoj Gupta

Received: 6 October 2022
Accepted: 27 October 2022
Published: 28 October 2022

Publisher's Note: MDPI stays neutral with regard to jurisdictional claims in published maps and institutional affiliations.

1. Introduction

Perovskite solar cells provide photoelectric conversion in wide wavelength ranges and exhibit excellent photovoltaic properties [1–6]. Since the thin films of $CH_3NH_3PbI_3$ ($MAPbI_3$) can be formed by a spin-coating method [7,8], there is the advantages of an easy production process and low cost. Despite these merits, there is a problem that the stability of the perovskite compound is extremely low because of desorption of CH_3NH_3 (MA), and the lead used in the perovskite layer is toxic [9–11]. On the other hand, the photovoltaic properties of perovskite solar cells have been reported to depend strongly on the compositions and crystal structures of the perovskite compounds [12–14]. Therefore, to solve these problems, studies have been conducted in which various elements are doped in a perovskite precursor solution [15–20].

Several studies on partial replacement of MA in $MAPbI_3$ by formamidinium ($HC(NH_2)_2$, FA) have been reported [21–27]. One of these studies reported that the conversion efficiency of $MAPbI_3$ perovskite solar cells decreased to 50% of the initial value within one month [28]. On the other hand, it was reported that the conversion efficiency of the FA-added device was maintained about 80% of the initial value within one month after the production. The addition of FA can be expected to improve the stability of the perovskite solar cells.

There are also studies using Sn as an alternative element to Pb because of its toxicity [29–32]. $MASnI_3$ is unstable in the atmosphere, and the Sn-added device fabricated in a nitrogen atmosphere has an initial conversion efficiency of 5.38% [33]. When the device was held in a nitrogen atmosphere for 24 h, the conversion efficiency was reduced to 1.94%, and it was difficult to maintain the conversion efficiency [33].

The purpose of this study is to fabricate and characterize tin (Sn)- and copper (Cu)-added perovskite solar cells, which were prepared by high temperature annealing at 190 °C in ambient air using decaphenylcyclopentasilane (DPPS). The addition of Sn and Cu can be expected to influence crystal growth of the perovskite grains, which would lead to increase the short-circuit current density [34–36]. Although the annealing temperatures for the fabrication of the $MAPbI_3$ perovskite layers are commonly 100 °C, this low-temperature

annealing might cause instability. Since high-temperature annealing could be effective for the formation of more stable perovskites, hot air-blowing [37,38] and higher temperature annealing in ambient air using DPPS [39,40] were applied in the present work. The DPPS layer is expected to work as a protective layer and a hole transport layer on the perovskite layer. The effects of Sn- and Cu-additions to the perovskite crystals on the photovoltaic properties were investigated using light-induced current density-voltage (*J*-*V*) measurements, external quantum efficiency, X-ray diffraction (XRD), optical microscopy, and first-principle calculation.

2. Materials and Methods

A schematic illustration showing the fabrication processes used to fabricate photovoltaic cells is shown in Figure 1. All processes were performed in air [41,42]. F-doped tin oxide (FTO, Nippon Sheet Glass Company, Ltd., Tokyo, Japan) substrates were cleaned in an ultrasonic bath with acetone and ethanol, and dried under nitrogen gas. Subsequently, the FTO substrates were treated with an ultraviolet ozone cleaner (ASM401N, Asumi Giken, Tokyo, Japan) for 15 min.

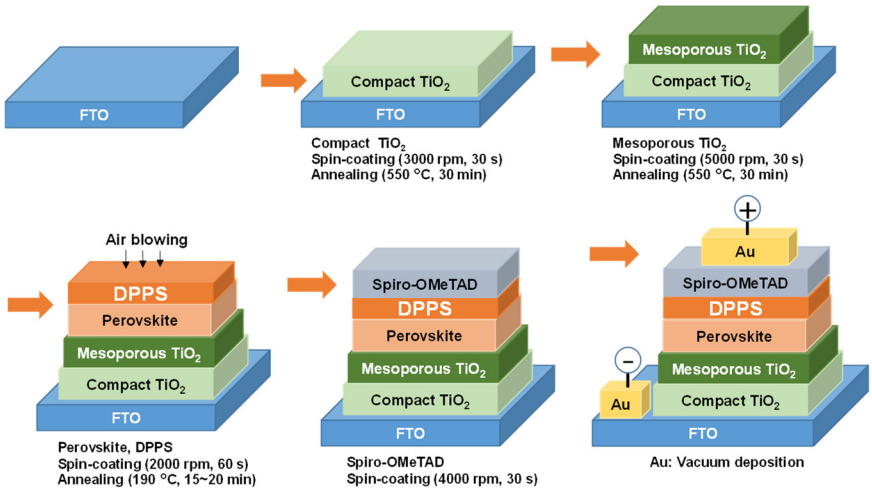

Figure 1. Schematic illustration of the process used to fabricate the present photovoltaic cells.

TiO_x precursor solutions (0.15 and 0.30 M) were prepared from titanium diisopropoxide bis(acetyl acetonate) (Sigma Aldrich, Tokyo, Japan) and 1-butanol (Fujifilm Wako Pure Chemical Corporation, Osaka, Japan). Both TiO_x precursor solutions were spin-coated onto the FTO substrate at 3000 rpm for 30 s (MSA100, Mikasa, Tokyo, Japan) and annealed at 125 °C for 5 min, however, the 0.30 M precursor was spin-coated twice to form a uniform layer. After that, the FTO substrate was sintered at 550 °C for 30 min to form a compact TiO_2 layer. A mesoporous TiO_2 layer was spin-coated on top of the compact TiO_2 layer at 5000 rpm for 30 s using TiO_2 paste. The TiO_2 paste was prepared using TiO_2 powder (P-25, Aerosil, Tokyo, Japan, 100 mg) and poly(ethylene glycol) (PEG, Nacalai Tesque, Kyoto, Japan, #20000, 10 mg) in distilled water (0.5 mL). This solution was mixed with acetylacetone (Fujifilm Wako Pure Chemical Corporation, 10 µL) and the surfactant Triton X-100 (Sigma Aldrich, 5 µL) for 30 min and was then allowed to stand for ~24 h to suppress bubble formation within the solution. The FTO substrates with the TiO_2 were annealed at 550 °C for 30 min to form the mesoporous TiO_2 layer.

The perovskite compounds were prepared by mixing solutions of CH_3NH_3I (Tokyo Chemical Industries, Tokyo Japan), $HC(NH_2)_2I$ (FAI, Tokyo Chemical Industries), $PbCI_2$ (Sigma Aldrich), and $SnCl_2$ (Fujifilm Wako Pure Chemical Corporation), CuBr (Sigma Aldrich), at 70 °C. Formamidinium [$HC(NH_2)_2$] (FA) with a larger ionic radius than MA was added to improve the stability [43,44]. All materials were dissolved in *N*,*N*-dimethylformamide (Sigma Aldrich).

Standard $MAPbI_3$ precursors with molar concentrations of MAI and $PbCl_2$ of 2.4 and 0.8 M, respectively, were prepared, and $MA_{0.9}FA_{0.1}Pb_{0.98}Sn_{0.02}I_3$, $MA_{0.9}FA_{0.1}Pb_{0.98}Sn_{0.01}Cu_{0.01}I_3$, $MA_{0.9}FA_{0.1}Pb_{0.96}Sn_{0.02}Cu_{0.02}I_3$, $MA_{0.9}FA_{0.1}Pb_{0.94}Sn_{0.02}Cu_{0.04}I_3$, precursors were also prepared, as summarized in Table 1. The chemical reaction of 3MAI + $PbCl_2$ → $MAPbI_3$ + 2MACl (↑) was used in the present work [37], and the MACl was vaporized during annealing. To stabilize the perovskite structure, FA was co-added when Sn and Cu were added to the crystals. As the FAI, Sn, and Cu composition increased, the tolerance factor (*t*-factor) [14] increased a little, indicating that the crystals have similar stabilities from the viewpoint of *t*-factors. The perovskite precursor solutions were spin-coated at 2000 rpm for 60 s and applied an air-blowing method during spin-coating [37]. The perovskite precursor solution was spin-coated three times, and DPPS was added dropwise during the third spin coating (45 s after the start). The DPPS solutions were prepared from decaphenylcyclopentasilane (SI-30–15, Osaka Gas Chemical, Osaka, Japan) and chlorobenzene (Fujifilm Wako Pure Chemical Corporation) [39,40]. The thickness of the DPPS layer was about 10 nm. The device was annealed at 190 °C for 15 min in the ambient air.

Table 1. Compositions and calculated *t*-factors of the present $MA_{0.9}FA_{0.1}Pb_{1-x-y}Sn_xCu_yI_3$ perovskite compounds.

Device Notation	Sn (%)	Cu (%)	*t*-Factor
Standard	0	0	0.9115
Sn 2%	2	0	0.9209
Sn 1% + Cu 1%	1	1	0.9213
Sn 2% + Cu 2%	2	2	0.9235
Sn 2% + Cu 4%	2	4	0.9262

The hole-transport layer was deposited by spin-coating. A chlorobenzene solution (0.5 mL) of 2,2′,7,7′-tetrakis-(*N*,*N*-di-p-methoxyphenylamine)-9,9′-spirobifluorene (spiro-OMeTAD, Fujifilm Wako Pure Chemical Corporation, 36.1 mg) was prepared by mixing it for 12 h. An acetonitrile solution (0.5 mL) of lithium bis (trifluoromethylsulfonyl) imide (Li-TFSI, Tokyo Chemical Industry) was also prepared by mixing it for 12 h. A mixture solution of the spiro-OMeTAD solution with 4-tertbutylpridine (14.4 µL, Sigma Aldrich) and Li-TFSI solution (8.8 µL) was prepared by mixing it at 70 °C for 30 min. The spiro-OMeTAD layer was deposited by spin-coating at 4000 rpm for 30 s. After that, gold (Au) thin film electrodes were deposited as electrodes by using a resistance heating type vacuum evaporation system (SVC-700TM, Sanyu Electron, Co., Ltd., Tokyo, Japan).

The *J*-*V* characteristics (B2901A, Keysight, Santa Rosa, CA, USA) of the photovoltaic cells were measured when illuminated with a solar simulator (XES-301S, San-ei Electric, Osaka, Japan) at 100 mW cm^{-2} with an air mass 1.5. The solar cells were illuminated through the side of the FTO substrates, and the exposed area was 0.080 cm^2. Three electrodes were measured for each device, and the maximum and minimum values were indicated as error bars. The EQEs of the solar cells were also measured by an incident photon to electron conversion efficiency measurement system (QE-R, Enli Technology, Kaohsiung, Taiwan). The microstructures of the perovskite layers were investigated by an X-ray diffractometer (D2 PHASER, Bruker, Billerica, MA, USA), while the surface morphologies of the perovskite layers were examined using an optical microscope (Eclipse E600, Nikon, Tokyo, Japan).

The ab initio quantum calculations used the Vanderbilt ultra-soft pseudo-potentials, scalar relativistic generalized gradient approximations, and the Perdew–Burke–Ernzerhof exchange–correlation function and density functional theory (Quantum Espresso, version 5.2.1, Quantum Espresso Foundation, Cambridge, UK). The initial parameters used for the crystal were 2 × 2 × 2 supercells, the kinetic energy cut-off for the wave functions of 25 Ry, and the charge density of 225 Ry.

3. Results and Discussion

The photovoltaic properties of perovskite-based solar cells were investigated using the *J-V* curves obtained under illumination. The *J-V* curves of the solar cells featuring FAI 10% + Sn 2%, FAI 10% + Sn 1% + Cu 1%, FAI 10% + Sn 2% + Cu 2%, and FAI 10% + Sn 2% + Cu 4% incorporated $MAPbI_3$ perovskites are presented in Figure 2a. The photovoltaic parameters, namely open-circuit voltages (V_{OC}), short-circuit current densities (J_{SC}), fill factor (FF), series resistance (R_s), shunt resistance (R_{sh}), photoconversion efficiency (η), averaged photoconversion efficiency (η_{ave}) and the energy gap (E_g) of all analyzed cells are listed in Table 2. The E_g values decreased by adding Sn, which also corresponded to the previous study [33].

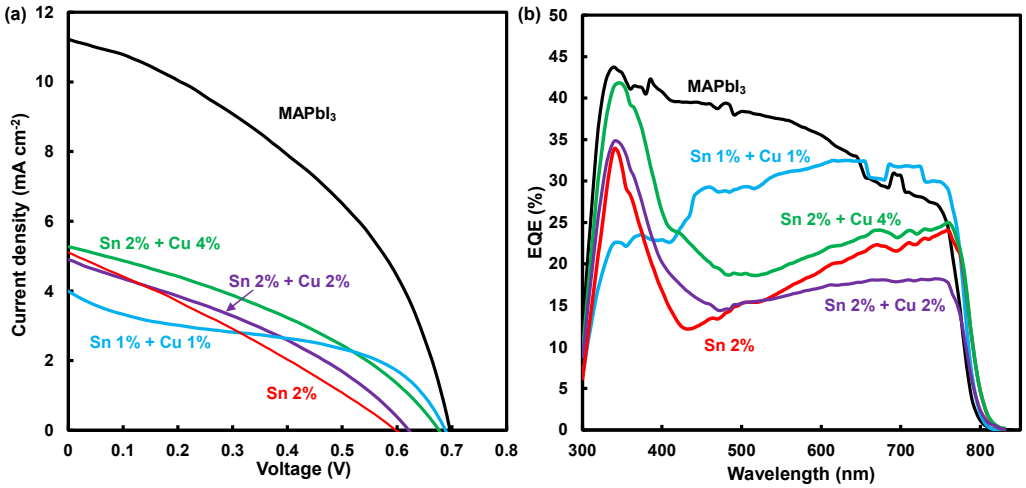

Figure 2. (**a**) *J-V* characteristics and (**b**) EQE of the present perovskite solar cells.

Table 2. Compositions and calculated *t*-factors of the present $MA_{0.9}FA_{0.1}Pb_{1-x-y}Sn_xCu_yI_3$ perovskite compounds.

Device	J_{SC} (mA cm^{-2})	V_{OC} (V)	FF	R_S (Ω cm^2)	R_{Sh} (Ω cm^2)	η (%)	η_{ave} (%)	E_g (eV)
Standard	11.2	0.696	0.419	16.2	217	3.28	2.13	1.57
Sn 2%	5.12	0.598	0.287	68.7	149	0.879	0.546	1.54
Sn 1% + Cu 1%	4.00	0.688	0.427	24.8	586	1.17	0.802	1.55
Sn 2% + Cu 2%	4.91	0.621	0.342	47.8	200	1.04	0.653	1.54
Sn 2% + Cu 4%	5.28	0.677	0.364	42.8	245	1.30	1.02	1.54

Addition of $SnCl_2$, and CuBr to $MA_{0.9}FA_{0.1}PbI_3$ perovskite affected the photovoltaic parameters, and the J_{SC}, V_{OC}, FF, and η values of the Sn-added cells were lower than those of the standard device. When 1%, 2%, and 4% CuBr were co-added to $MAPbI_3$ perovskite, the η values of the cells increased.

The external quantum efficiencies (EQEs), which is the ratio of the number of charge carriers collected by the solar cell to the number of incident photons, of the devices including FAI, $SnCl_2$, and CuBr are shown in Figure 2b. The addition of FAI or $SnCl_2$ to the $MAPbI_3$ perovskite expanded the region of EQE to 400–840 nm. Energy gaps (E_g) were calculated from the EQE spectra, and are listed in Table 2. The E_g values of Sn-added and Sn/Cu-added perovskites were lower than that of the standard $MAPbI_3$ crystal.

The changes in η and J_{SC} of perovskite solar cells were investigated at 25 °C and 20% humidity for about 200 days, as shown in Figure 3. For the $MAPbI_3$ solar cell, both η and J_{SC} decreased after 203 days. The degradation would be due to the decrease in photocurrent by carrier recombination around defects which were formed by diffusion of MA cations and halogen anions for the long-term period.

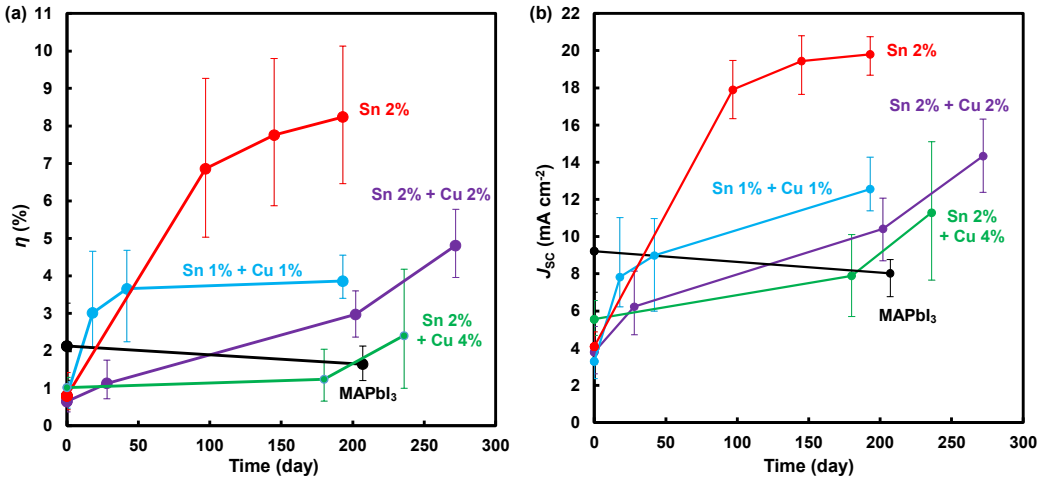

Figure 3. Changes of (**a**) photoelectric conversion efficiencies, and (**b**) short-circuit current densities.

For the 10% FA and 2% Sn-added device, both η and J_{SC} increased after 193 days. The increase in J_{SC} and η would be due to promotion of carrier diffusion in the perovskite crystals. The co-addition of FA and Sn would facilitate the solid-phase reaction with diffusion in the perovskite layer. On the other hand, slow deterioration behavior was observed for the standard $MAPbI_3$ device.

J-V characteristics and photovoltaic parameters of each device with the best efficiency for the time course are summarized in Figure 4 and Table 3. Sn 2% added device provided the best efficiencies in the present work. Since several devices showed small increases of efficiencies, their long-term performances were also investigated, as listed in Table 4. Although efficiencies of Sn-added devices decreased, device with Sn 2% + Cu 2% showed better stability than Sn 2% device.

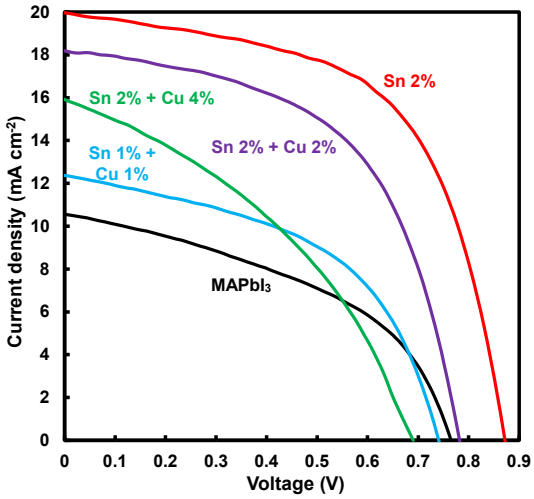

Figure 4. *J-V* characteristics of each device with the best efficiency for the time course.

Perovskite solar cells without FA and DPPS layer were also investigated, and the photovoltaic parameters are listed in Table 5. The compositions of the perovskite compounds were $CH_3NH_3Pb_{0.95}Sn_{0.05}I_3$ and $CH_3NH_3Pb_{0.9}Sn_{0.05}Cu_{0.05}I_3$, which are denoted as Sn 5% and Sn 5% + Cu 5%, respectively. Since there was no DPPS layer, the annealing temperature of the perovskite layers was 140 °C for 10 min. For the Sn-added device, both η and J_{SC} increased after 115 days, which agreed with the results of Figure 3, indicating the effectiveness of Sn addition.

Table 3. Photovoltaic parameters of the perovskite solar cells with the best photoconversion efficiencies.

Device	Time (Day)	J_{SC} (mA cm^{-2})	V_{OC} (V)	FF	R_S (Ω cm^2)	R_{Sh} (Ω cm^2)	η (%)	η_{ave} (%)
Standard	0	11.2	0.696	0.419	16.2	217	3.28	2.13
Sn 2%	193	20.0	0.871	0.583	6.14	323	10.14	8.24
Sn 1% + Cu 1%	193	12.4	0.740	0.499	9.38	217	4.56	3.86
Sn 2% + Cu 2%	386	18.2	0.781	0.550	7.36	345	7.81	7.23
Sn 2% + Cu 4%	236	15.1	0.712	0.389	16.9	107	4.17	2.77

Table 4. Photovoltaic parameters of the present perovskite solar cells after long times.

Device	Time (Day)	J_{SC} (mA cm^{-2})	V_{OC} (V)	FF	R_S (Ω cm^2)	R_{Sh} (Ω cm^2)	η (%)	η_{ave} (%)
Sn 2%	817	16.3	0.823	0.514	4.61	287	6.90	6.55
Sn 1% + Cu 1%	818	6.57	0.747	0.541	2.56	442	2.65	2.44
Sn 2% + Cu 2%	680	15.8	0.761	0.587	3.35	375	7.04	6.34
Sn 2% + Cu 4%	660	14.1	0.471	0.270	4.95	37.8	1.79	1.38

Table 5. Photovoltaic parameters of the perovskite solar cells without FA and DPPS layer.

Device	Time (Day)	J_{SC} (mA cm^{-2})	V_{OC} (V)	FF	R_S (Ω cm^2)	R_{Sh} (Ω cm^2)	η (%)	η_{ave} (%)
Sn 5%	0	3.00	0.704	0.344	65.7	357	0.724	0.432
Sn 5%	83	8.17	0.894	0.560	10.3	613	4.10	3.25
Sn 5%	115	11.60	0.922	0.577	7.53	564	6.16	5.84
Sn 5% + Cu 5%	0	1.82	0.360	0.322	67.8	420	0.211	0.170
Sn 5% + Cu 5%	76	11.6	0.750	0.457	13.1	192	3.96	2.84
Sn 5% + Cu 5%	115	10.75	0.788	0.384	22.7	229	3.25	2.88

Optical microscopy images of the present solar cells are shown in Figure 5, and the particle sizes and surface coverages of the perovskite crystals are summarized in a part of Table 6. The average particle sizes were measured from dark regions of the image, and the surface coverage was calculated from the histogram of the contrast by using an image software (Adobe, Photoshop). Lattice constants and 100 crystal orientation in Table 6 were measured from XRD data in Figure 6, which will be described later. The particle size and surface coverage of the $MAPbI_3$ perovskite incorporated with 2% Sn increased from 5.45 μm to 7.68 μm and from 67.95 to 93.35, respectively, after 193 days. On the other hand, for the solar cell featuring pristine $MAPbI_3$ perovskite, the particle size and surface coverage decreased from 6.77 μm to 6.46 μm and from 75.65 to 68.05, respectively.

Table 6. Structural parameters of the present perovskite crystals. I_{100}/I_{210}: ratios of (100) diffraction intensities (I_{100}) to (210) diffraction intensities (I_{210}).

Device	Time (Days)	Lattice Constant (Å)	I_{100}/I_{210}	Grain Size (μm)	Coverage (%)	K (10^{-19} m^2 s^{-1})
Standard	0	6.271(1)	2.5	6.77	75.6	
	203	6.269(1)	2.1	6.46	68.0	−2.34
Sn 2%	0	6.280(1)	2.4	5.45	67.9	
	193	6.270(1)	2.6	7.68	93.3	17.6
Sn 2% + Cu 2%	0	6.282(1)	2.3	5.06	75.5	
	283	6.277(0)	3.7	7.57	86.7	13.0

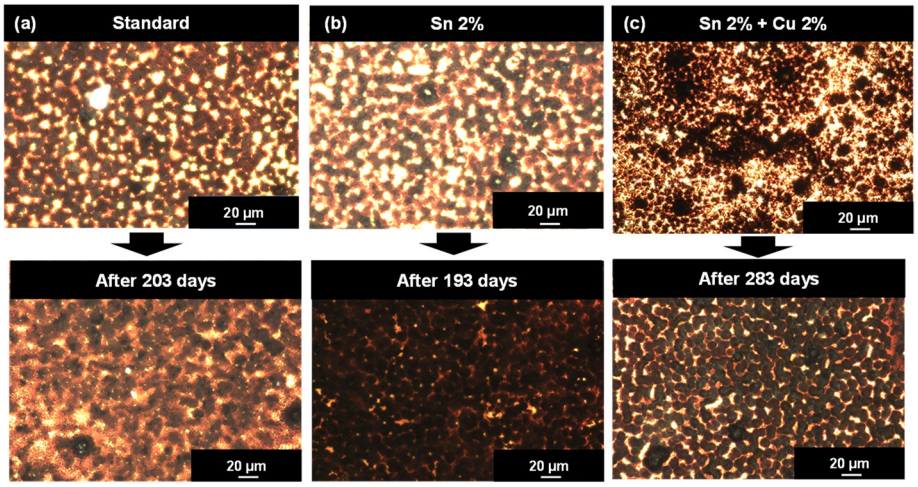

Figure 5. Optical microscope images of the devices.

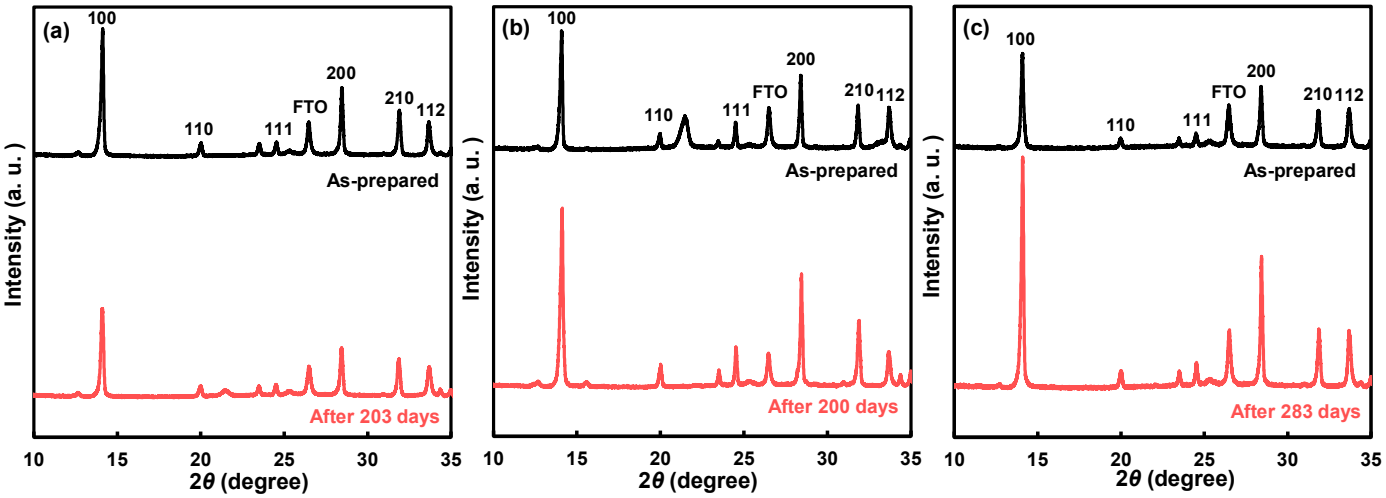

Figure 6. Changes of XRD patterns of (**a**) standard, (**b**) Sn 2%, and (**c**) Sn 2% + Cu 2% devices.

XRD patterns and lattice constants (a) of the standard, +Sn, and +Sn + Cu devices are shown in Figure 6 and Table 6. An intensity of the 100 peak for the Sn 2% added device increased after 200 days, and the crystal orientation of the I_{100}/I_{210} ratio increased from 2.4 to 2.6, as listed in Table 6. This indicates crystal growth of (100)-oriented perovskite grains after 200 days. In comparison, the I_{100}/I_{210} ratio for the standard device decreased from 2.5 to 2.1. An intensity ratio of the 100 peak (I_{100}) to 210 peak (I_{210}) for the Sn 2% + Cu 2% added device increased further to 3.7 after 283 days. Addition of a small amount of Sn and Cu improved the crystal orientation and suppressed the grain boundaries in the perovskite layer. The crystal growth in the perovskite layer would reduce the trap density between perovskite grains and increase the J_{SC} and η [36].

Figure 7a,b are schematic illustrations of crystal growth of the perovskites and the ionic diffusion in the perovskite, respectively. It is considered that MA and I were desorbed by annealing the perovskite layer during device fabrication. The energy derived from these lattice defects would cause ionic diffusion, which would promote grain growth. Then, the surface coverage and crystal orientation are improved, resulting in an increase in short-circuit current density and conversion efficiency [45–48].

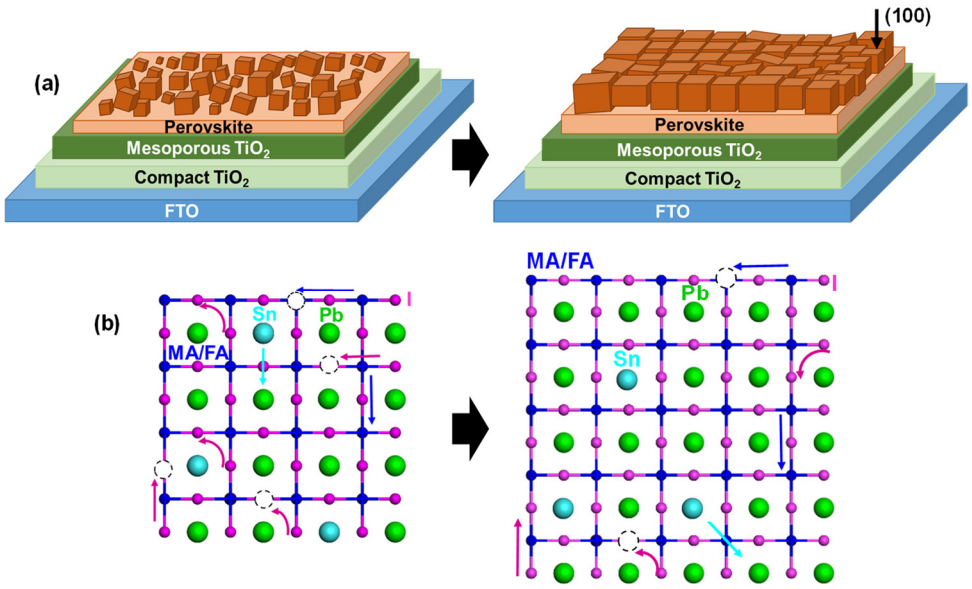

Figure 7. Schematic illustration of (**a**) crystal growth and (**b**) the ionic diffusion in perovskite crystals.

Growth rates of perovskite grains for the devices were compared. The initial grain size of the crystal is d_0 (m), the material/temperature-dependent constant is K (m^2 s^{-1}), the constant is n, and the temperature retention time is t_r (s). The crystal grain size was d (m), and the constant K was calculated using the following formula $d^n - d_0^n = Kt_r$, and listed in Table 6. The n changes depending on the variable, and the n was set as 2 because of a single perovskite layer. d and d_0 values were determined from the particle sizes. The K values for the standard and Sn/Cu added systems negative and positive, respectively.

Activation energies of ionic diffusions of MA^+, Pb^{2+}, and I^- are 0.84 eV, 2.31 eV, and 0.58 eV, respectively [49]. The Pb ion has the largest activation energy for ionic diffusion in this crystal, and crystal growth of $MAPbI_3$ at room temperature might be suppressed by the difficulty of the Pb diffusion. Since Sn and Cu have smaller ionic radii than Pb, the Sn and Cu ions would have smaller activation energy for diffusion, which could contribute to the crystal growth even by the room temperature aging, as observed in the XRD patterns of Figure 6.

The added Sn^{2+} can be easily oxidized into Sn^{4+}, which would act as non-radiative recombination centers, degrading solar cell performance. However, the perovskite device with a small amount of Sn showed improvement of the performance in the present work, and high temperature annealing might be related with this device stability.

In addition to the device characterization, the partial density of states (PDOS), total density of states (TDOS) and electron density distribution were investigated by first-principles calculation [50–55]. The structure models of $MAPbI_3$ and $MA(FA)Pb(Sn)I_3$ used for the calculations are shown in Figure 8a,b, and the PDOS are shown in Figure 8c,d, respectively. The PDOS of Sn/FA doped perovskite is different from that of the standard $MAPbI_3$, especially around the conduction band. For the $MAPbI_3$, the p-orbital of Pb is dominant around the conduction band, whereas the p-orbital of Sn is dominant for the $MA(FA)Pb(Sn)I_3$. Bandgap energies of the $MAPbI_3$ and $MA(FA)Pb(Sn)I_3$ were calculated as 1.382 and 1.178 eV, respectively, which agree with the results obtained in the experimental system.

Calculation results of electron density distribution for the $MAPbI_3$ and $MA(FA)Pb(Sn)I_3$ are shown in Figure 8e,f, respectively. Positions of nitrogen (N) are indicated in Figure 8e. The electron density distribution of I was widened, and the electrons in the vicinity of Sn were delocalized in the $MA(FA)Pb(Sn)I_3$. Addition of Sn would promote carrier flow, which lead to the improvement of the short-circuit current density.

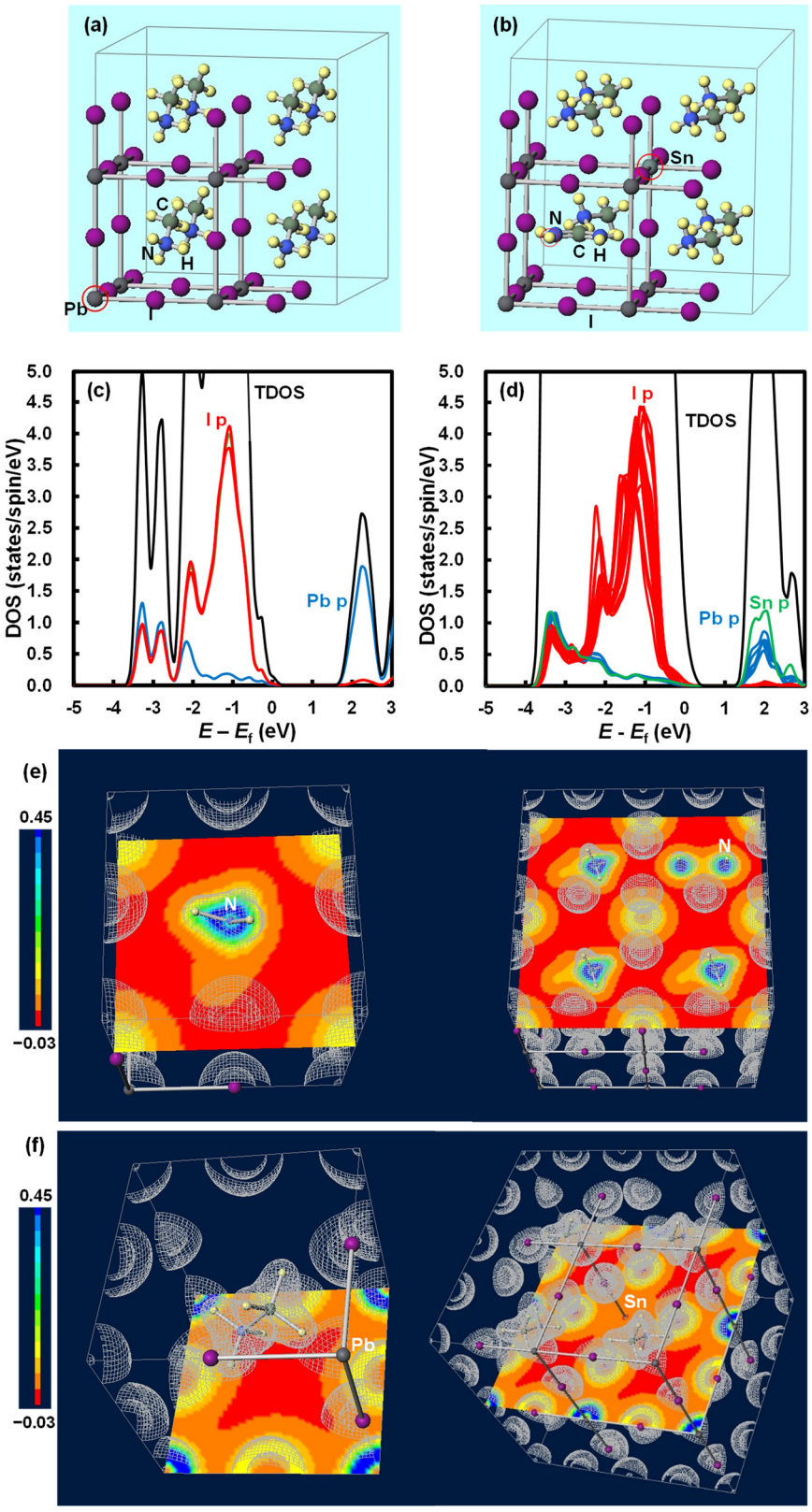

Figure 8. Crystal structures of (**a**) $MAPbI_3$ and (**b**) MA(FA)Pb(Sn)I_3, (**c**) partial density of state of $MAPbI_3$, (**d**) partial density of state of MA(FA)Pb(Sn)I_3, electron density distribution of (**e**) $MAPbI_3$, and (**f**) MA(FA)Pb(Sn)I_3.

4. Conclusions

Solar cells using perovskite in the photoactive layer were fabricated by using a spin-coating technique in ordinary air, and the influences on photovoltaic characteristics by adding Sn and Cu to the perovskite compounds were investigated. Addition of Sn to the $MAPbI_3$ perovskite crystals improved the long-term photovoltaic properties owing to the crystal growth and improvement of (100) crystal orientation of the perovskite layer. The Cu addition with Sn also enhanced the (100) orientation. The partial substitution of Pb^{2+} in the perovskite crystals by Sn^{2+} ions affected charge transfer via hybridization between the p orbitals of I and Sn.

Author Contributions: Conceptualization, Y.A., T.O. and M.K.; Data curation, Y.A., T.O. and M.K.; Formal analysis, Y.A., T.O., M.K., A.S. and R.O.; Funding acquisition, T.O.; Investigation, Y.A., T.O., M.K. and R.O.; Methodology, Y.A., T.O., M.K. and A.S.; Project administration, T.O.; Resources, M.O., S.F., T.T. and T.H.; Writing—original draft, Y.A. and T.O.; Writing—review and editing, Y.A., T.O., M.K., A.S., R.O., M.O., S.F., T.T. and T.H. All authors have read and agreed to the published version of the manuscript.

Funding: This research was partly funded by Japan Society for the Promotion of Science as a Grant-in-Aid for Scientific Research (C) 21K04809.

Institutional Review Board Statement: Not applicable.

Informed Consent Statement: Not applicable.

Data Availability Statement: Data is contained within the article.

Conflicts of Interest: The authors declare no conflict of interest.

References

1. Zhou, H.; Chen, Q.; Li, G.; Luo, S.; Song, T.B.; Duan, H.S.; Hong, Z.; You, J.; Liu, Y.; Yang, Y. Interface engineering of highly efficient perovskite solar cells. *Science* **2014**, *345*, 542–546. [CrossRef] [PubMed]
2. Miyasaka, T. Perovskite photovoltaics: Rare functions of organo lead halide in solar cells and optoelectronic devices. *Chem. Lett.* **2015**, *44*, 720. [CrossRef]
3. Saliba, M.; Orlandi, S.; Matsui, T.; Aghazada, S.; Cavazzini, M.; Correa-Baena, J.-P.; Gao, P.; Scopelliti, R.; Mosconi, E.; Dahmen, K.H.; et al. A molecularly engineered hole-transporting material for efficient perovskite solar cells. *Nat. Energy* **2016**, *1*, 15017. [CrossRef]
4. Li, X.; Bi, D.; Yi, C.; Décoppet, J.D.; Luo, J.; Zakeeruddin, S.M.; Hagfeldt, A.; Grätzel, M. A vacuum flash–assisted solution process for high-efficiency large-area perovskite solar cells. *Science* **2016**, *353*, 58–62. [CrossRef] [PubMed]
5. Chen, Z.; Turedi, B.; Alsalloum, A.Y.; Yang, C.; Zheng, X.; Gereige, I.; AlSaggaf, A.; Mohammed, O.F.; Bakr, O.M. Single-crystal $MAPbI_3$ perovskite solar cells exceeding 21% power conversion efficiency. *ACS Energy Lett.* **2019**, *4*, 1258–1259. [CrossRef]
6. Lee, J.; Baik, S. Enhanced crystallinity of CH3NH3PbI3 by the pre-coordination of PbI2–DMSO powders for highly reproducible and efficient planar heterojunction perovskite solar cells. *RSC Adv.* **2018**, *8*, 1005–1013. [CrossRef]
7. Eze, V.O.; Lei, B.; Mori, T. Air-assisted flow and two-step spin-coating for highly efficient CH3NH3PbI3 perovskite solar cells. *Jpn. J. Appl. Phys.* **2016**, *55*, 02BF08. [CrossRef]
8. Nishi, K.; Oku, T.; Kishimoto, T.; Ueoka, N.; Suzuki, A. Photovoltaic Characteristics of $CH_3NH_3PbI_3$ Perovskite Solar Cells Added with Ethylammonium Bromide and Formamidinium Iodide. *Coatings* **2020**, *10*, 410. [CrossRef]
9. Dunfield, S.P.; Bliss, L.; Zhang, F.; Luther, J.M.; Zhu, K.; van Hest, M.F.A.M.; Reese, M.O.; Berry, J.J. From defects to degradation: A mechanistic understanding of degradation in perovskite solar cell devices and modules. *Adv. Energy Mater.* **2020**, *10*, 1904054. [CrossRef]
10. Lee, J.W.; Kim, S.G.; Yang, J.M.; Yang, Y.; Park, N.G. Verification and mitigation of ion migration in perovskite solar cells. *APL Mater.* **2019**, *7*, 041111. [CrossRef]
11. Shi, Z.; Guo, J.; Chen, Y.; Li, Q.; Pan, Y.; Zhang, H.; Xia, Y.; Huang, W. Lead-free organic–inorganic hybrid perovskites for photovoltaic applications: Recent advances and perspectives. *Adv. Mater.* **2017**, *29*, 1605005. [CrossRef]
12. Saliba, M.; Matsui, T.; Seo, J.Y.; Domanski, K.; Baena, J.P.C.; Nazeeruddin, M.K.; Zakeeruddin, S.M.; Tress, W.; Abate, A.; Hagfeldt, A.; et al. Cesium-containing triple cation perovskite solar cells: Improved stability, reproducibility and high efficiency. *Energy Environ. Sci.* **2016**, *9*, 1989–1997. [CrossRef]
13. Yu, Y.; Wang, C.; Grice, C.R.; Shrestha, N.; Chen, J.; Zhao, D.; Liao, W.; Cimaroli, A.J.; Roland, P.J.; Ellingson, R.J.; et al. Improving the performance of formamidinium and cesium lead triiodide perovskite solar cells using lead thiocyanate additives. *ChemSusChem* **2016**, *9*, 3288–3297. [CrossRef]
14. Oku, T. Crystal structures of perovskite halide compounds used for solar cells. *Rev. Adv. Mater. Sci.* **2020**, *59*, 264–305. [CrossRef]

15. Wang, Y.; Dar, M.I.; Ono, L.K.; Zhang, T.; Kan, M.; Li, Y.; Zhang, L.; Wang, X.; Yang, Y.; Gao, X.; et al. Thermodynamically stabilized β-$CsPbI_3$–based perovskite solar cells with efficiencies >18%. *Science* **2019**, *365*, 591–595. [CrossRef]
16. McMeekin, D.P.; Sadoughi, G.; Rehman, W.; Eperon, G.E.; Saliba, M.; Hörantner, M.T.; Haghighirad, A.; Sakai, N.; Korte, L.; Rech, B.; et al. A mixed-cation lead mixed-halide perovskite absorber for tandem solar cells. *Science* **2016**, *351*, 151–155. [CrossRef]
17. Oku, T.; Ohishi, Y.; Suzuki, A. Effects of antimony addition to perovskite-type $CH_3NH_3PbI_3$ photovoltaic devices. *Chem. Lett.* **2016**, *45*, 134–136. [CrossRef]
18. Suzuki, A.; Kishimoto, K.; Oku, T.; Okita, M.; Fukunishi, S.; Tachikawa, T. Additive effect of lanthanide compounds into perovskite layer on photovoltaic properties and electronic structures. *Synth. Met.* **2022**, *287*, 117092. [CrossRef]
19. Enomoto, A.; Suzuki, A.; Oku, T.; Okita, M.; Fukunishi, S.; Tachikawa, T.; Hasegawa, T. Effects of Cu, K and guanidinium addition to $CH_3NH_3PbI_3$ perovskite solar cells. *J. Electron. Mater.* **2022**, *51*, 4317–4328. [CrossRef]
20. Okumura, R.; Oku, T.; Suzuki, A.; Okita, M.; Fukunishi, S.; Tachikawa, T.; Hasegawa, T. Effects of adding alkali metals and organic cations to Cu-based perovskite solar cells. *Appl. Sci.* **2022**, *12*, 1710. [CrossRef]
21. Zhao, Y.; Tan, H.; Yuan, H.; Yang, Z.; Fan, J.Z.; Kim, J.; Voznyy, O.; Gong, X.; Quan, L.N.; Tan, C.S.; et al. Perovskite seeding growth of formamidinium-lead iodide-based perovskites for efficient and stable solar cells. *Nat. Commun.* **2018**, *9*, 1607. [CrossRef]
22. Adjokatse, S.; Kardula, J.; Fang, H.H.; Shao, S.; ten Brink, G.H.; Loi, M.A. Effect of the device architecture on the performance of $FA_{0.85}MA_{0.15}PbBr_{0.45}I_{2.55}$ planar perovskite solar cells. *Adv. Mater. Interfaces* **2019**, *6*, 1801667. [CrossRef]
23. Yan, W.; Rao, H.; Wei, C.; Liu, Z.; Bian, Z.; Xin, H.; Huang, W. Highly efficient and stable inverted planar solar cells from $(FAI)_x(MABr)_{1-x}PbI_2$ perovskites. *Nano Energy* **2017**, *35*, 62–70. [CrossRef]
24. Tosado, G.A.; Zheng, E.; Yu, Q. Tuning cesium–guanidinium in formamidinium tin triiodide perovskites with an ethylenediammonium additive for efficient and stable lead-free perovskite solar cells. *Mater. Adv.* **2020**, *1*, 3507–3517. [CrossRef]
25. Kandori, S.; Oku, T.; Nishi, K.; Kishimoto, T.; Ueoka, N.; Suzuki, A. Fabrication and characterization of potassium- and formamidinium-added perovskite solar cells. *J. Ceram. Soc. Jpn.* **2020**, *128*, 805. [CrossRef]
26. Oku, T.; Kandori, S.; Taguchi, M.; Suzuki, A.; Okita, M.; Minami, S.; Fukunishi, S.; Tachikawa, T. Polysilane-inserted methylammonium lead iodide perovskite solar cells doped with formamidinium and potassium. *Energies* **2020**, *13*, 4776. [CrossRef]
27. Suzuki, A.; Taguchi, M.; Oku, T.; Okita, M.; Minami, S.; Fukunishi, S.; Tachikawa, T. Additive effects of methyl ammonium bromide or formamidinium bromide in methylammonium lead iodide perovskite solar cells using decaphenylcyclopentasilane. *J. Mater. Sci. Mater. Electron.* **2021**, *32*, 26449–26464. [CrossRef]
28. Maqsood, A.; Li, Y.; Meng, J.; Song, D.; Qiao, B.; Zhao, S.; Xu, Z. Perovskite solar cells based on compact, smooth $FA_{0.1}MA_{0.9}PbI_3$ film with efficiency exceeding 22%. *Nanoscale Res. Lett.* **2020**, *15*, 89. [CrossRef]
29. Li, M.; Wang, Z.K.; Zhuo, M.P.; Hu, Y.; Hu, K.H.; Ye, Q.Q.; Jain, S.M.; Yang, Y.G.; Gao, X.Y.; Liao, L.S. Pb–Sn–Cu ternary organometallic halide perovskite solar cells. *Adv. Mater.* **2018**, *30*, 1800258. [CrossRef]
30. Isikgor, F.H.; Li, B.; Zhu, H.; Xu, Q.; Ouyang, J. High performance planar perovskite solar cells with a perovskite of mixed organic cations and mixed halides, $MA_{1-x}FA_xPbI_{3-y}Cl_y$. *J. Mater. Chem. A* **2016**, *4*, 12543–12553. [CrossRef]
31. Elseman, A.M.; Shalan, A.E.; Sajid, S.; Rashad, M.M.; Hassan, A.M.; Li, M. Copper-substituted lead perovskite materials constructed with different halides for working $(CH_3NH_3)_2CuX_4$-based perovskite solar cells from experimental and theoretical view. *ACS Appl. Mater. Interfaces* **2018**, *10*, 11699–11707. [CrossRef] [PubMed]
32. Ueoka, N.; Oku, T.; Suzuki, A.; Sakamoto, H.; Yamada, M.; Minami, S.; Miyauchi, S. Fabrication and characterization of CH_3NH_3(Cs)Pb(Sn)I_3(Cl) perovskite solar cells with TiO_2 nanoparticle layers. *Jpn. J. Appl. Phys.* **2018**, *57*, 02CE03. [CrossRef]
33. Hao, F.; Stoumpos, C.C.; Cao, D.H.; Chang, R.P.H.; Kanatzidis, M.G. Lead-free solid-state organic–inorganic halide perovskite solar cells. *Nat. Photonics* **2014**, *8*, 489–494. [CrossRef]
34. Ueoka, N.; Oku, T.; Suzuki, A. Additive effects of alkali metals on Cu-modified $CH_3NH_3PbI_{3-\delta}Cl_\delta$ photovoltaic devices. *RSC Adv.* **2019**, *9*, 24231. [CrossRef] [PubMed]
35. Ueoka, N.; Oku, T. Effects of co-addition of sodium chloride and copper(ii) bromide to mixed-cation mixed-halide perovskite photovoltaic devices. *ACS Appl. Energy Mater.* **2020**, *9*, 24231. [CrossRef]
36. Ueoka, N.; Oku, T.; Suzuki, A. Effects of doping with Na, K, Rb, and formamidinium cations on $(CH_3NH_3)_{0.99}Rb_{0.01}Pb_{0.99}Cu_{0.01}I_{3-x}$ (Cl, Br)$_x$ perovskite photovoltaic cells. *AIP Adv.* **2020**, *10*, 125023. [CrossRef]
37. Oku, T.; Ohishi, Y.; Ueoka, N. Highly (100)-oriented $CH_3NH_3PbI_3$(Cl) perovskite solar cells prepared with NH_4Cl using an air blow method. *RSC Adv.* **2018**, *8*, 10389–10395. [CrossRef]
38. Oku, T.; Ohishi, Y. Effects of annealing on $CH_3NH_3PbI_3$ (Cl) perovskite photovoltaic devices. *J. Ceram. Soc. Jpn.* **2018**, *126*, 56–60. [CrossRef]
39. Taguchi, M.; Suzuki, A.; Oku, T.; Ueoka, N.; Minami, S.; Okita, M. Effects of annealing temperature on decaphenylcyclopentasilane-inserted $CH_3NH_3PbI_3$ perovskite solar cells. *Chem. Phys. Lett.* **2019**, *737*, 136822. [CrossRef]
40. Oku, T.; Taguchi, M.; Suzuki, A.; Kitagawa, K.; Asakawa, Y.; Yoshida, S.; Okita, M.; Minami, S.; Fukunishi, S.; Tachikawa, T. Effects of polysilane addition to chlorobenzene and high temperature annealing on $CH_3NH_3PbI_3$ perovskite photovoltaic devices. *Coatings* **2021**, *11*, 665. [CrossRef]
41. Suzuki, A.; Kato, M.; Ueoka, N.; Oku, T. Additive effect of formamidinium chloride in methylammonium lead halide compound-based perovskite solar cells. *J. Electron. Mater.* **2019**, *48*, 3900–3907. [CrossRef]
42. Oku, T.; Zushi, M.; Imanishi, Y.; Suzuki, A.; Suzuki, K. Microstructures and photovoltaic properties of perovskite-type $CH_3NH_3PbI_3$ compounds. *Appl. Phys. Express* **2014**, *7*, 121601. [CrossRef]

43. Jokar, E.; Chien, C.H.; Tsai, C.M.; Fathi, A.; Diau, E.W.G. Robust tin-based perovskite solar cells with hybrid organic cations to attain efficiency approaching 10%. *Adv. Mater.* **2019**, *37*, 1804835. [CrossRef] [PubMed]
44. Kim, G.; Min, H.; Lee, K.S.; Lee, D.Y.; Yoon, S.M.; Seok, S.I. Impact of strain relaxation on performance of α-formamidinium lead iodide perovskite solar cells. *Science* **2020**, *370*, 108–112. [CrossRef]
45. Yang, W.S.; Park, B.W.; Jung, E.H.; Jeon, N.J.; Kim, Y.C.; Lee, D.U.; Shin, S.S.; Seo, J.; Kim, E.K.; Noh, J.H.; et al. Iodide management in formamidinium-lead-halide–based perovskite layers for efficient solar cells. *Science* **2017**, *356*, 1376–1379. [CrossRef]
46. Konstantakou, M.; Stergiopoulos, T. A critical review on tin halide perovskite solar cells. *J. Mater. Chem. A* **2017**, *5*, 11518–11549. [CrossRef]
47. Ferdani, D.W.; Pering, S.R.; Ghosh, D.; Kubiak, P.; Walker, A.B.; Lewis, S.E.; Johnson, A.L.; Baker, P.J.; Islam, M.S.; Cameron, P.J. Partial cation substitution reduces iodide ion transport in lead iodide perovskite solar cells. *Energy Environ. Sci.* **2019**, *12*, 2264–2272. [CrossRef]
48. Osherov, A.; Feldman, Y.; Ashiri, I.K.; Cahen, D.; Hodes, G. Halide diffusion in $MAPbX_3$: Limits to topotaxy for halide exchange in perovskites. *Chem. Mater.* **2020**, *32*, 4223–4231. [CrossRef]
49. Eames, C.; Frost, J.M.; Barnes, P.R.F.; O'Regan, B.C.; Walsh, A.; Islam, M.S. Ionic transport in hybrid lead iodide perovskite solar cells. *Nat. Commun.* **2015**, *6*, 7497. [CrossRef]
50. Suzuki, A.; Oe, M.; Oku, T. Fabrication and characterization of Ni-, Co-, and Rb-incorporated $CH_3NH_3PbI_3$ perovskite solar cells. *J. Electron. Mater.* **2021**, *50*, 1980–1995. [CrossRef]
51. Suzuki, A.; Oku, T. Effects of mixed-valence states of Eu-doped $FAPbI_3$ perovskite crystals studied by first-principles calculation. *Mater. Adv.* **2021**, *2*, 2609–2616. [CrossRef]
52. Suzuki, A.; Kitagawa, K.; Oku, T.; Okita, M.; Fukunishi, S.; Tachikawa, T. Additive effects of copper and alkali metal halides into methylammonium lead iodide perovskite solar cells. *Electron. Mater. Lett.* **2022**, *18*, 176–186. [CrossRef]
53. Kishimoto, T.; Oku, T.; Suzuki, A.; Ueoka, N. Additive effects of guanidinium iodide on $CH_3NH_3PbI_3$ perovskite solar cells. *Phys. Status Solidi A* **2021**, *218*, 2100396. [CrossRef]
54. Ono, I.; Oku, T.; Suzuki, A.; Asakawa, Y.; Terada, S.; Okita, M.; Fukunishi, S.; Tachikawa, T. Fabrication and characterization of $CH_3NH_3PbI_3$ solar cells with added guanidinium and inserted with decaphenylpentasilane. *Jpn. J. Appl. Phys.* **2022**, *61*, SB1024. [CrossRef]
55. Terada, S.; Oku, T.; Suzuki, A.; Okita, M.; Fukunishi, S.; Tachikawa, T.; Hasegawa, T. Ethylammonium bromide- and potassium-added $CH_3NH_3PbI_3$ perovskite solar cells. *Photonics* **2022**, *9*, 791. [CrossRef]